The Astrophysical Journal, 650:252–260, 2006 October 10

IMPRINT OF GRAVITATIONAL LENSING BY POPULATION III STARS IN GAMMA-RAY BURST LIGHT CURVES

Y. Hirose,[1] M. Umemura,[1] A. Yonehara,[2,3] and J. Sato[1]
Received 2005 May 1; accepted 2006 May 18

ABSTRACT

We propose a novel method of extracting the imprint of gravitational lensing by Population III stars in the light curves of gamma-ray bursts (GRBs). Significant portions of GRBs can originate in hypernovae of Population III stars and be gravitationally lensed by foreground Population III stars or their remnants. If the lens mass is on the order of $10^2-10^3\ M_\odot$ and the lens redshift is greater than 10, the time delay between two lensed images of a GRB is $\approx$1 s and the image separation is $\approx$10 μas. Although it is difficult to resolve the two lensed images spatially with current facilities, the light curves of the two images are superimposed with a delay of $\approx$1 s. GRB light curves usually exhibit noticeable variability, where each spike is less than 1 s. If a GRB is lensed, all spikes are superimposed with the same time delay. Hence, if the autocorrelation of the light curve with changing time interval is calculated, it should show resonance at the time delay of the lensed images. Applying this autocorrelation method to GRB light curves that are archived as the BATSE catalog, we demonstrate that more than half of the light curves show recognizable resonance they are lensed. Furthermore, in 1821 GRBs we actually find one candidate for a GRB lensed by a Population III star, which may be located at redshift 20–200. The present method is quite straightforward and therefore provides an effective tool for searching for Population III stars at redshift greater than 10. Using this method, we may find more candidates for GRBs lensed by Population III stars in the data of the *Swift* satellite.

Subject headings: gamma rays: bursts — gravitational lensing

1. INTRODUCTION

The recent observation of the cosmic microwave background by the *Wilkinson Microwave Anisotropy Probe* (*WMAP*) suggests that the reionization of the universe took place at redshifts of $8 \lesssim z \lesssim 14$ (Spergel et al. 2003, 2006; Kogut et al. 2003; Page et al. 2006). This result implies that first-generation stars (Population III stars) were possibly born at $z \gtrsim 10$ if UV photons emitted from Population III stars are responsible for cosmic reionization. However, there is no direct evidence that Population III stars actually formed at $z > 10$. Obviously, it is impossible with current or near future facilities to detect the emission from a Population III star at such high redshifts (e.g., Mizusawa et al. 2004). However, gamma-ray bursts (GRBs) can be detected even at $z > 10$ if they arise there. GRBs are the only currently available tool for probing first-generation objects in the universe. If one uses absolute magnitude data of GRBs with known redshifts, one can expect more than half of $z > 10$ GRBs to be detectable (Lamb & Reichart 2000). Roughly 3000 GRBs have been detected to date, but redshifts have been measured for only 30 GRBs (Bloom et al. 2003), among which the most distant is GRB 000131 at $z = 4.5$ (Andersen et al. 2000). However, if empirical relations between the spectral properties and the absolute magnitude are used, the GRBs detected to date may include events at $z > 10$ (Lloyd-Ronning et al. 2002; Yonetoku et al. 2004; Murakami et al. 2005). In addition, recently a new GRB satellite, *Swift*, has been launched (Gehrels et al. 2004). *Swift* is now accumulating more GRB data at a high rate. Recently, GRB 050904, detected by *Swift*, in terms of metal absorption lines and Lyman break, turns out to have occurred at $z = 6.295$ (Kawai et al. 2006).

The discovery of the association between GRB 030329 and SN 2003dh has demonstrated that at least a portion of long bursts in GRBs are caused by the collapse of massive stars (Kawabata et al. 2003; Price et al. 2003; Uemura et al. 2003). On the other hand, Population III stars are expected to form in a top-heavy fashion with the peak at $10^2-10^3\ M_\odot$ in the initial mass function (IMF; e.g., Nakamura & Umemura 2001 and references therein). In addition, the theoretical study by Heger & Woosley (2002) suggests that Population III stars of between 100 and 140 $M_\odot$ may end their lives as GRBs accompanied by core collapse into black holes. Heger et al. (2003) estimate, assuming the IMF by Nakamura & Umemura (2001), that 5% of Population III stars can result in GRBs. In the context of a cold dark matter cosmology, more than 10%–30% of GRBs are expected to occur at $z \gtrsim 10$, assuming that the redshift distributions of GRBs trace the cosmic star formation history (Bromm & Loeb 2002). Thus, the observed GRBs highly probably include GRBs originating from Population III stars at $z \gtrsim 10$.

The firm methods to measure redshifts are the detection of absorption and/or emission lines of host galaxies of GRBs (e.g., Metzger et al. 1997) or the Lyα absorption edge in afterglow (Andersen et al. 2000). However, these methods cannot be applied for all GRBs but have been successful in determining redshifts for only 30 GRBs (Bloom et al. 2003). Instead, some empirical laws have been applied to many more GRBs. They include the variability-luminosity relation (Fenimore & Ramirez-Ruiz 2000), the lag-luminosity relation (Norris et al. 2000), the E_p-luminosity relation (Amati et al. 2002), and the spectral peak energy–to–luminosity relation (Yonetoku et al. 2004). Applying these relations to GRBs, the redshift distributions of GRBs are derived (Fenimore & Ramirez-Ruiz 2000; Norris et al. 2000; Schaefer et al. 2001; Lloyd-Ronning et al. 2002; Yonetoku et al. 2004). Some analyses conclude that a portion of GRBs are located at $z \gtrsim 10$. However, it is still controversial whether such an indirect technique is correct or not.

In this paper, we propose a novel method of constraining the redshifts of GRBs that may originate from Population III stars at

[1] Center for Computational Sciences, University of Tsukuba, Ibaraki 305-8577, Japan.
[2] Department of Physics, University of Tokyo, Hongo, Bunkyo, Tokyo 113-0033, Japan.
[3] Astronomisches Rechen-Institut, Zentrum für Astronomie, Universität Heidelberg, Mönchhofstrasse 12-14, 69120 Heidelberg, Germany.

$z \gtrsim 10$. In this method, the effects of gravitational lensing by Population III stars are considered. The lensing of GRBs was considered for the first time by Paczyński (1986, 1987), who proposed the possibility that a soft gamma-ray repeater is produced by gravitational lensing of a single burst at a cosmological distance. In addition, Loeb & Perna (1998) first discussed the microlensing effect of GRB afterglows, and Garnavich et al. (2000) found a candidate microlensed afterglow (GRB 000301C). The rates of such events are further discussed from theoretical points of view (Koopmans & Wambsganss 2001; Wyithe & Turner 2002; Baltz & Hui 2005). Blaes & Webster (1992) argue for the method of detecting cosmological clumped dark matter by using the probability of detectable GRB lensing. Nemiroff et al. (1993) and Marani et al. (1999) search for a compact dark matter candidate using actual GRB data obtained by the Burst and Transient Source Experiment (BATSE) on the *Compton Gamma Ray Observatory* satellite. They focus on large-mass lenses of up to $10^6\ M_\odot$, which cause a delay timescale of several tens to 100 s. On the other hand, Williams & Wijers (1997) investigate the influence on the GRB light curve of the millisecond gravitational lensing caused by each star in a lensing galaxy. In addition, Nemiroff & Marani (1998) argue that it is possible to place constraints on the cosmic density of dark matter, baryons, stars, and so on by microlensing by stellar mass objects. In the present method, we focus on gravitational lensing by Population III stars. If the mass of Population III stars is on the order of 10^2–$10^3\ M_\odot$ and the redshift is greater than 10, the time delay between two lensed images of a GRB is $\approx$1 s. Quite advantageously, this time delay is longer than the time resolution (64 ms) of GRB light curves and shorter than the duration of GRB events, which is several tens to 100 s for long bursts. Thus, we can see the superimposed light curves of two lensed images. This method seeks the imprint of gravitational lensing by Population III stars in GRB light curves. We attempt to extract the imprint of lensing by calculating the autocorrelation of light curves.

In this paper, we assume standard ΛCDM cosmological parameters: $H_0 = 70$ km s^{-1} Mpc^{-1}, $\Omega_M = 0.3$, $\Omega_\Lambda = 0.7$, and $\Omega_b = 0.04$. The paper is organized as follows: In § 2, the formalism of the gravitational lensing and the estimation of the time delay between the two images are provided. In § 3, the method of finding the evidence of lensing by Population III stars is proposed. In addition, we demonstrate the potentiality of the present method for artificially lensed GRBs and describe how to determine the redshifts of lensed GRBs. In § 4, we apply this method to BATSE data of 1821 GRBs and find a candidate lensed GRB. Section 5 is devoted to the conclusions.

2. GRAVITATIONAL LENSING

We consider a GRB lensed by a foreground Population III star. Here we presuppose the lens model of a point mass. The Einstein ring radius gives a typical scale of gravitational lensing, which is expressed as

$$\theta_{\rm E} \equiv \left(\frac{4GM_L}{c^2}\frac{D_{LS}}{D_{OS}D_{OL}}\right)^{1/2}, \tag{1}$$

where G is the gravity constant, c is the speed of light, M_L is the mass of a lens object, and D_{LS}, D_{OS}, and D_{OL} are the angular diameter distances between the lens and the source, the observer and the source, and the observer and the lens, respectively. A point-mass lens produces two images with angular directions of

$$\theta = \frac{\beta}{2}\left[1 \pm \sqrt{1 + 4\left(\frac{\theta_{\rm E}}{\beta}\right)^2}\right], \tag{2}$$

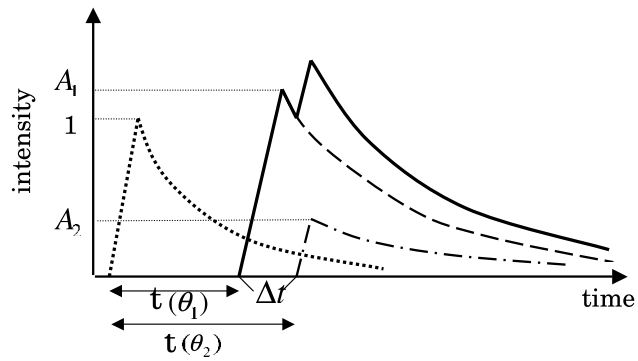

FIG. 1.—Schematic diagram of lensed GRB light curve. The dotted line represents the original light curve, while the dashed and dot-dashed lines represent the light curves of image 1 and image 2, respectively. The superimposed light curve of lensed images is shown by the solid line. The intensities are normalized by the maximum intensity of the original light curve.

where β is the angle of the lens from the line of sight to the source. We hereafter refer to the image with $\theta > \theta_{\rm E}$ as image 1 and that with $\theta < \theta_{\rm E}$ as image 2. The brightnesses of images 1 and 2 are respectively magnified by

$$A_{1,2} = \frac{1}{4}[(1 + 4f^{-2})^{1/2} + (1 + 4f^{-2})^{-1/2} \pm 2], \tag{3}$$

where $f = \beta/\theta_{\rm E}$. Thus, image 1 is brighter than the original one, while image 2 is fainter. In the case of a lens of a Population III star, the Einstein radius is estimated as

$$\theta_{\rm E} \simeq 10\left(\frac{M_L}{10^3\ M_\odot}\right)^{1/2}\left(\frac{\tilde{D}}{4\times 10^4\ {\rm Mpc}}\right)^{-1/2}\ \mu{\rm as}, \tag{4}$$

where $\tilde{D} \equiv D_{OS}D_{OL}/D_{LS}$. Obviously, this angular separation is impossible to resolve by current facilities. Hence, we can just observe the superposition of two images.

However, the light curves of the two images are superimposed with a time delay caused by the gravitational lensing, as shown in Figure 1. The arrival time of signals for a lensed image is expressed as

$$t(\theta) = \frac{(1+z_L)}{c}\frac{D_{OS}D_{OL}}{D_{LS}}\left[\frac{1}{2}(\theta-\beta)^2 - \Psi(\theta)\right], \tag{5}$$

where z_L is the redshift of the lens object and Ψ is the so-called lens potential. For the point-mass lens model, Ψ is expressed as

$$\Psi(\theta) = \frac{D_{LS}}{D_{OS}D_{OL}}\frac{4GM_L}{c^2}\ \ln\left|\frac{\theta}{\theta_C}\right|, \tag{6}$$

where θ_C is constant (Narayan & Bartelmann 1999). Then, the time delay between two images is given by

$$\Delta t(z_L, M_L, f) = t(\theta_2) - t(\theta_1) \propto M_L(1+z_L). \tag{7}$$

It should be noted that Δt is determined solely by the mass and redshift of the lens, regardless of the source redshift. In other words, the time delay places a constraint just on the lens, not on the source. However, if the lens redshift (z_L) is determined, it gives the minimum value of the source redshift (z_S), since z_S must be higher than z_L.

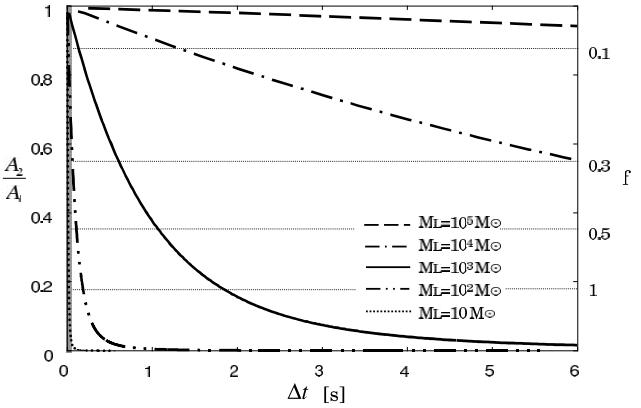

FIG. 2.—Relation between the time delay and the magnification ratio (A_2/A_1) between two images. The redshift of the lens object is fixed to 50. The curves show lens masses of $10-10^5\ M_\odot$ with an increment of 1 order of magnitude. The right vertical axis, $f = \beta/\theta_E$, is also shown corresponding to the magnification ratio. The time resolution of BATSE data, $\Delta t = 64$ ms, is represented by the gray region at the left edge of the plot.

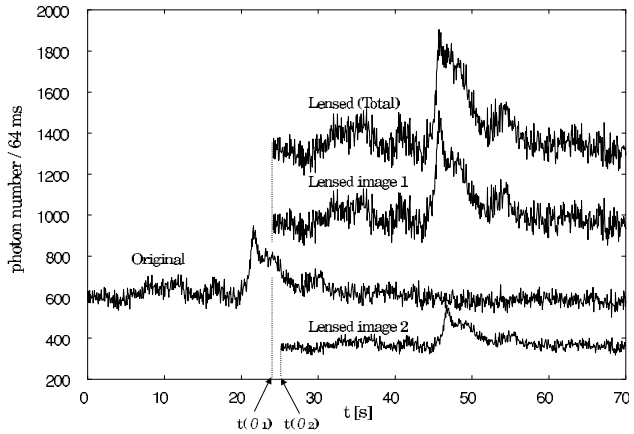

FIG. 3.—Original light curve of GRB 930214 obtained by BATSE and artificially lensed light curves. The lens is assumed to be a Population III star with $M_L = 10^3\ M_\odot$ at $z_L = 50$, while the source is located at $z_S = 51$. Lensed image 1, image 2, and the total light curves are shown. The time delay between two images is $\Delta t = 1.0$ s under the assumption of $f = 0.5$.

Figure 2 illustrates the relation between the time delay Δt and the magnification ratio between image 1 and image 2, assuming a lens redshift of 50. This figure shows that a lens with $\gtrsim 10^4\ M_\odot$ yields a time delay longer than the standard GRB duration if the typical delay timescale is assessed by $f \approx 1$. (Note that, as shown below, if f becomes larger than unity, the ratio of magnification becomes smaller and therefore the contribution of image 2 becomes difficult to extract. Also, if f becomes smaller than unity, the probability of lensing goes down.) On the other hand, a lens with $<10\ M_\odot$ leads to Δt shorter than the time resolution of the light curves, and therefore the information about the delay is buried. The mass scale of $10^2-10^3\ M_\odot$ expected for Population III stars gives $10^{-1}\ \mathrm{s} \lesssim \Delta t \lesssim 1$ s, which is longer than the time resolution and shorter than the GRB duration. Hence, this mass range appears to be suitable for extracting the time delay information.

However, the actual GRB light curves generally exhibit variabilities with timescales shorter than Δt. Thus, it is not straightforward to extract the time delay information. To demonstrate this difficulty, we show the light curve of GRB 930214 and the artificially lensed light curve in Figure 3, where $M_L = 10^3\ M_\odot$, $z_L = 50$, and $f = 0.5$ are assumed. The time delay is $\Delta t = 1.0$ s in this case. This figure clearly shows that if we observe only the superimposed lensed light curve, it seems impossible to recognize by appearance that this light curve is lensed. Hence, we invoke a new technique to discriminate a lensed GRB from an unlensed one.

3. AUTOCORRELATION METHOD

3.1. *Theory*

We pay attention to the fact that all spikes in a light curve are individually lensed. Then, many pairs with a time separation of Δt appear in the light curve, as schematically shown in Figure 4*b*. To detect those pairs, we employ the autocorrelation method (e.g., Geiger & Schneider 1996). The autocorrelation, $C(\delta t)$, is defined as

$$C(\delta t) = \frac{\sum_i I(t_i + \delta t) I(t_i)}{\sum_i I(t_i)^2}, \qquad (8)$$

where $I(t_i)$ is the number of photons contained in the ith bin in the GRB light curve. If there are pairs with Δt, autocorrelation (8) is expected to show a resonance "bump" around Δt, as shown in Figure 4*c*. Then we can evaluate the time delay by the existence of this bump.

3.2. *Robustness*

The autocorrelation method is simple and well defined, but the issue we should check is its applicability for actual GRB light curves. To test the robustness of this method, we produce artificially lensed light curves for GRBs in BATSE archived data and calculate the autocorrelation. We use 1821 light curves in the BATSE catalog with the time resolution of 64 ms.[4] Unless otherwise specified, we adopt the data of T_{90}, where T_{90} is defined by the duration such that the cumulative photon counts increase from 5% to 95% of the total GRB photon counts (Kouveliotou et al. 1993; Koshut et al. 1996). Then the summation in equation (8) is taken in the range of $T_{90}-\delta t$. However, if the data at T_{90} start with bins whose time resolution is worse than 1024 ms, we neglect those low-resolution bins.

In Figure 5, the resulting autocorrelation is shown for 10 GRB light curves. In each panel, a thin solid line represents the autocorrelation for the original light curve, while a thick solid line represents the autocorrelation for the artificially lensed light curve, where $M_L = 10^3\ M_\odot$, $z_L = 50$, and $f = 0.5$ are assumed, the same as in Figure 3, and therefore the time delay of lensed images is $\Delta t = 1$ s. We can see that there is no bump in $C(\delta t)$ for the original light curve, whereas a bump emerges around $\delta t = 1$ s in $C(\delta t)$ for the artificially lensed light curve. Note that $C(\delta t)$ for the artificially lensed light curve is stronger than $C(\delta t)$ for all of the original light curve, owing to the amplification by gravitational lensing; $C(\delta t)$ for the artificially lensed light curve is fit by a polynomial of eighth degree. Using the best-fit polynomial $F(\delta t)$, we define the dispersion, σ, of the autocorrelation curve by $\sigma^2 = \sum_{j=1}^{n} [C(\delta t_j) - F(\delta t_j)]^2/n$, where n is the number of bins. The levels of $\pm 3\ \sigma$ are shown by dashed lines. The zoomed view around the bump of $C(\delta t)$ for the artificially lensed light curve is also shown in each inset. For these GRBs, bumps exceeding 3 σ appear if lensed, corresponding to the time delay between two lensed images, Δt.

3.3. *Dependence on f*

In fact, not all GRB light curves exhibit bumps in $C(\delta t)$ when lensed. The fraction of GRBs that show bumps exceeding 3 σ in

[4] http://cossc.gsfc.nasa.gov/batse/BATSE_Ctlg/duration.html.

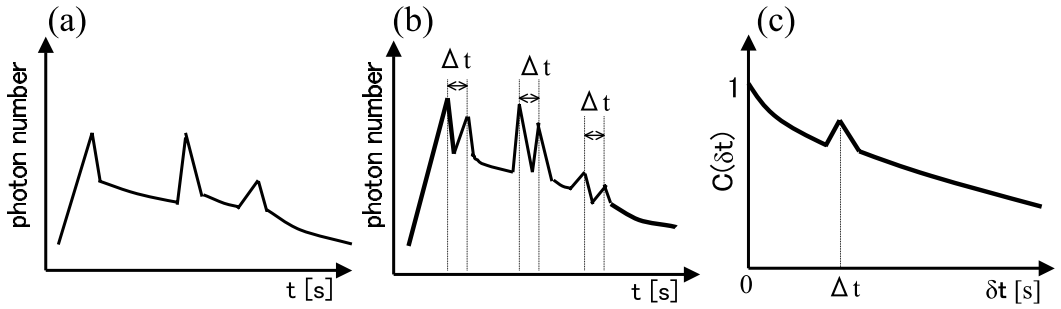

FIG. 4.—(*a*) Schematic of a spiky GRB light curve. (*b*) Light curve as the superposition of two lensed light curves with time delay of Δt. (*c*) Autocorrelation function calculated for light curve (*b*).

$C(\delta t)$ depends on the value of $f = \beta/\theta_{\rm E}$. In addition, the time delay Δt and the magnification $A_{1,2}$ depend on f. To demonstrate this, we show the dependence on f of the autocorrelation for the artificially lensed light curve of GRB 930214 in Figure 6. It is clear that if f is larger, the bump is suppressed. This is because the contribution of image 2 becomes smaller with increasing f. In this GRB, the bump over 3 σ disappears at $f > 1.0$. The value of f at which the bump disappears differs in each GRB. Using data of 220 GRBs, which are used in Fenimore & Ramirez-Ruiz (2000), we obtain the fraction of GRBs that show bumps over 3 σ in $C(\delta t)$ as a function of f. In this analysis, $\Delta t = 1.0$ s is assumed. The resulting fraction is shown in Figure 7*a*. For $f = 0.5$, about one-half of GRBs show bumps exceeding 3 σ in $C(\delta t)$. In contrast, the cross section of the gravitational lensing is proportional to f^2, which is also shown in Figure 7*a*. We evaluate the probability density of GRBs exhibiting bumps over 3 σ by multiplying the fraction of bump for which a bump appears by f^2. The normalized probability density against f is shown in Figure 7*b*. As a result, the probability is peaked around $f = 1$ and the standard deviation corresponds to $\Delta f \approx 0.25$. Note that this probability density is found to be hardly dependent on the value of Δt.

3.4. *Bump Detection Probability*

First, we estimate the optical depth of gravitational lensing by Population III stars. If we assume that a fraction α of baryonic matter composes Population III stars at $z \geq z_{\rm III}$, then the optical depth for $f \leq 1$ is given by

$$\tau(z_S) = \int_{z_{\rm III}}^{z_S} n_L(z_L)\sigma_L \frac{cdt}{dz_L}\, dz_L, \tag{9}$$

where σ_L is the cross section in the Einstein ring radius, $\sigma_L = \pi(D_{OL}\theta_{\rm E})^2$, and $n_L(z_L)$ is the number density of the lens objects given as

$$n_L(z_L) = \alpha \frac{3H_0^2}{8\pi G}\frac{\Omega_b}{M_L}(1+z_L)^3. \tag{10}$$

Then, the optical depth (9) is calculated as

$$\tau(z_S) = \frac{3}{5}\alpha\Omega_b \left\{ \left[\frac{(1+z_S)^{5/2}+1}{(1+z_S)^{5/2}-1}\right] \ln(1+z_S) - \left[\frac{(1+z_{\rm III})^{5/2}+1}{(1+z_{\rm III})^{5/2}-1}\right] \ln(1+z_{\rm III}) \right\} \tag{11}$$

in an Einstein–de Sitter universe (Turner et al. 1984; Turner & Umemura 1997). Here we assume $\alpha = 0.1$ and $z_{\rm III} = 10$. The resulting optical depth of Population III star lensing is shown in Figure 8. Using $\tau(z_S)$, we estimate the bump detection probability. Since $\tau(z_S)$ is the optical depth that a source is located inside the Einstein ring radius ($f \leq 1$), the differential optical depth that f is in the range of $[f, f+df]$ is given by $d[\tau(z_S)f^2] = \tau(z_S)df^2 = \tau(z_S)2fdf$. Hence, using the probability of a bump appearing, $p(f)$, shown in Figure 7*a*, the probability of bump detection is given by

$$P(z_S) = \int_0^\infty p(f)\tau(z_S)2f\, df. \tag{12}$$

The resulting bump detection probability is also shown in Figure 8. From this figure, the probability turns out to be $\approx$0.001 for $z_S = 20$–40. If we take into account that more than 10%–30% of GRBs occur at $z \gtrsim 10$ (Bromm & Loeb 2002), the number of bump detections expected for lensed GRBs is assessed to be one in a few thousand GRBs.

4. A CANDIDATE FOR A GRB LENSED AT $z \approx 60$

4.1. *Data Analysis*

As shown above, the autocorrelation of intrinsic light curves exhibits no bumps for almost all GRBs. However, a few in 1000 GRBs might show bumps in $C(\delta t)$ even for intrinsic light curves. Hence, we calculate the autocorrelation of all GRB light curves available in the BATSE catalog, which amount to 1821 GRBs. As a result, we have found one candidate, GRB 940919 (BATSE trigger No. 3174), in which a 3 σ bump in $C(\delta t)$ appears. The light curve and the autocorrelation of this GRB are shown in Figure 9. As seen in Figure 9*b*, a bump exceeding 3 σ appears at $\Delta t = 0.96$ s.

4.2. *Statistical Significance*

To check the statistical significance of the bump in $C(\delta t)$ of GRB 940919, we make a test with mock light curves. Here we generate mock light curves using a smoothed correlation function that dose not show any bump, and we investigate whether bumps appear in correlation functions just from pure statistical fluctuations.

From the Wiener-Khinchin theorem, the power spectra of light curves are given by

$$|I(\omega)|^2 = \mathcal{F}\left[\sum_i I(t_i)I(t_i+\delta t)\right], \tag{13}$$

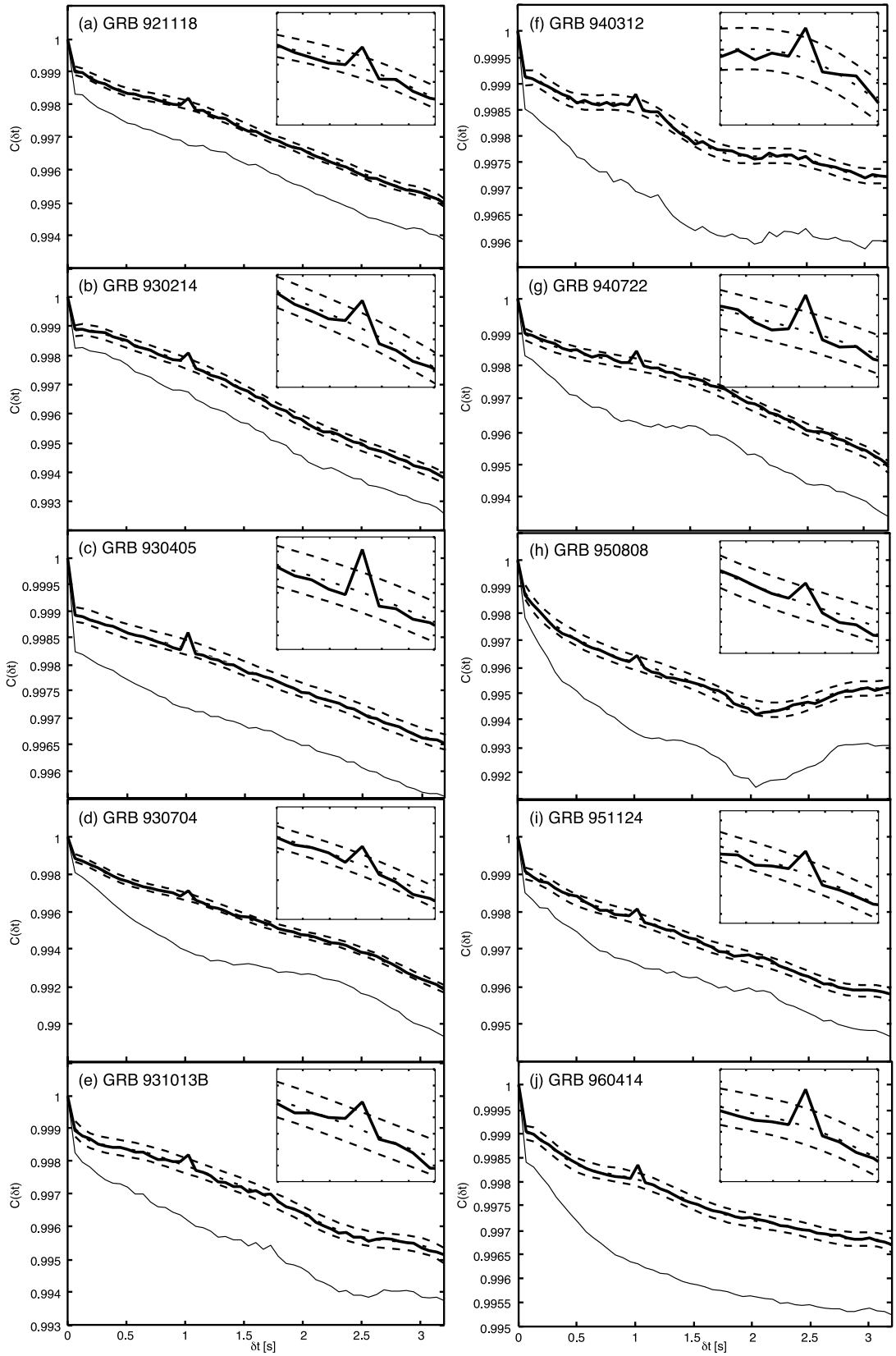

FIG. 5.—Autocorrelation against δt for 10 GRB light curves. In each panel, a thin curve shows the autocorrelation for the original light curve, while a thick curve shows that for the artificially lensed light curve. Here $M_L = 10^3\ M_\odot$, $z_L = 50$, and $f = 0.5$ are assumed, and therefore the time delay of lensed images is $\Delta t = 1$ s. A dotted curve is the best fit for the autocorrelation for lensed light curves, and two dashed curves show the $\pm 3\ \sigma$ level from the best fit. In each panel, a zoomed view around a correlation bump is also shown.

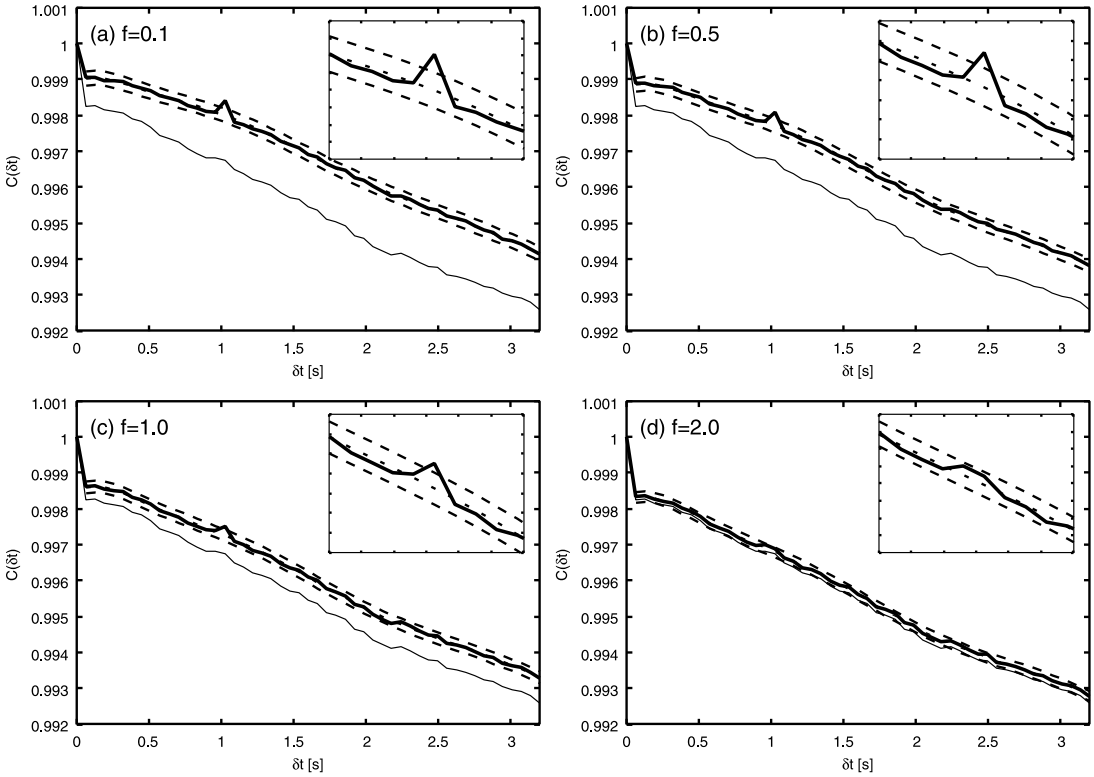

FIG. 6.—Dependence on $f = \beta/\theta_{\rm E}$ of the autocorrelation for the artificially lensed light curve of GRB 930214, which is the same GRB as in Fig. 5*b*. The time delay is $\Delta t = 0.1$ s. The meanings of the curves are the same as in Fig. 5. It is seen that the bump is weaker for larger *f*.

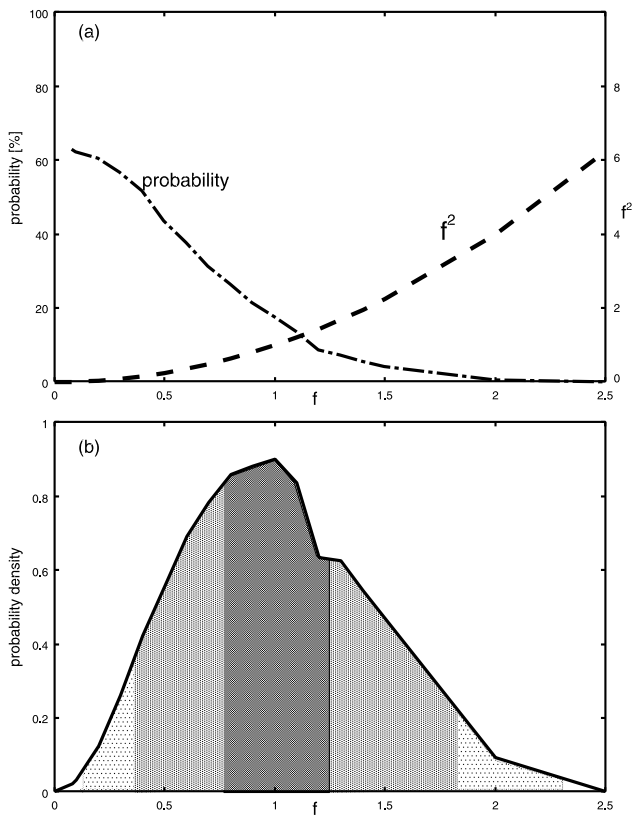

FIG. 7.—(*a*) Probability (*dot-dashed curve*) of exhibiting bumps exceeding 3 σ. Here $\Delta t = 1.0$ s is assumed. The dashed line shows f^2, which is proportional to the cross section of the gravitational lens. (*b*) Probability density of exhibiting bumps against *f*. The gray scale represents 1 σ, 2 σ, and 3 σ around $f = 1$ (*from dark to light*).

where $\mathcal{F}$ denotes the Fourier transformation and $\omega = 2\pi/\delta t$. We can generate mock light curves by the inverse Fourier transformation of $I(\omega)$. Here in order to add fluctuation to $I(\omega)$, we take random Gaussian distributions, where $|I(\omega)|$ is the standard deviation and the phase is random in the range of $[0, 2\pi]$. Then the mock light curve is given by

$$\tilde{I}(t) = \mathcal{F}^{-1}[I(\omega)] = \sum_{\omega} |\tilde{I}(\omega)| \cos(-\phi - \omega t), \qquad (14)$$

where $\tilde{I}(\omega)$ is a random sample in the Gaussian distribution and ϕ is the random phase shift from 0 to 2π. We produce 2000 mock light curves using a correlation function and recalculate

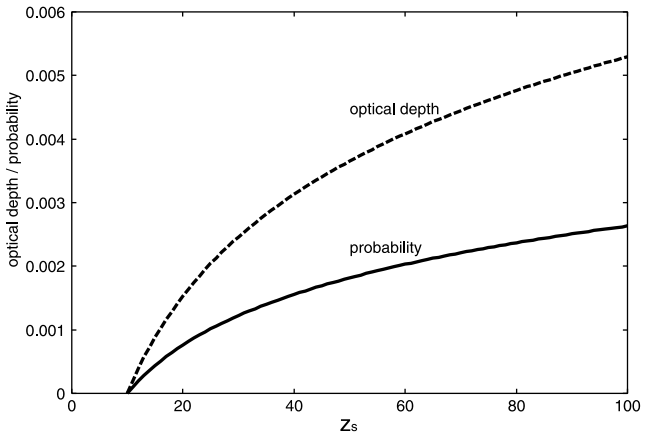

FIG. 8.—Probability (*solid line*) of bump detection for lensed GRBs. The dashed line shows the optical depth of gravitational lensing when a GRB source object is located at $z_S \geq 10$ and 10% of Ω_b at $z_L \geq 10$ contributes to gravitational lensing as a lens object.

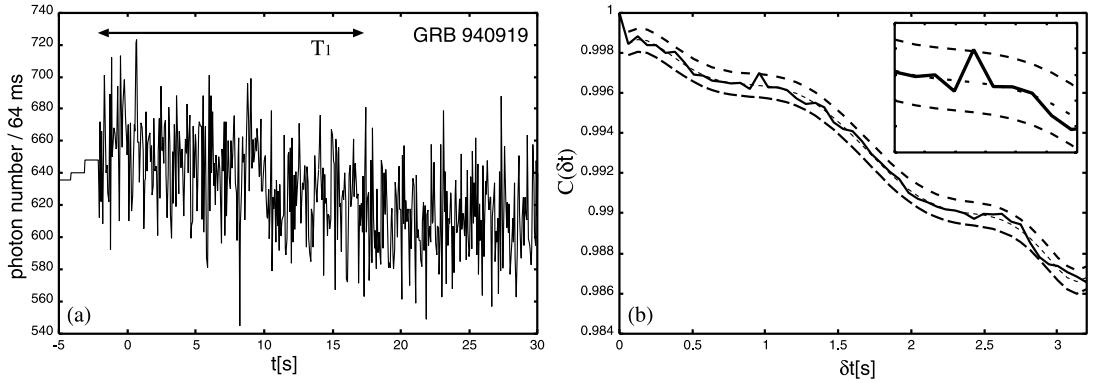

FIG. 9.—(*a*) Intrinsic light curve of GRB 940919. (*b*) Autocorrelation vs. δt. A 3 σ bump appears at $\Delta t = 0.96$ s.

the autocorrelation $C(\delta t)$ with equation (8). As a result, we have found that no bump higher than 3 σ appears in the $C(\delta t)$ of the 2000 mock light curves. A portion of the recalculated $C(\delta t)$ are shown in Figure 10. Thus, it is unlikely that a bump in the correlation arises as a result of pure statistical fluctuations.

4.3. *Light-Curve Decomposition*

As a further test for the lensing of the GRB 940919 light curve, we attempt to decompose the light curve, assuming that it is the superposition of two lensed light curves with $\Delta t = 0.96$ s, and analyze the decomposed light curves. The decomposition is performed with the following recurrence formula:

$$I_{\rm tot}(t) = I_1(t) + I_2(t), \tag{15}$$

$$I_2(t) = \frac{A_2}{A_1} I_1(t - \Delta t), \tag{16}$$

where $I_{\rm tot}(t)$ is the observed intensity, and $I_1(t)$ and $I_2(t)$ are the intensities for images 1 and 2, respectively. If these two equations are combined, $I_1(t)$ can be expressed by

$$I_1(t) = \sum_{j=0}^{N} \left(-\frac{A_2}{A_1} \right)^j I_{\rm tot}(t - j\Delta t). \tag{17}$$

The summation is taken in the range of $t - j\Delta t \geq 0$, where $t = 0$ is the starting point of T_{90}. Then we can also derive $I_2(t)$ with equation (15). In Figure 11, the decomposed light curves are shown in the case of $f = 1$, which is the most probable case as shown in § 3.3. The application of this decomposition method to the finite amount of data does not guarantee that the light curve is successfully decomposed into two lensed light curves. Hence, to check the validity of this decomposition method, we calculate the cross-correlation of two decomposed light curves by

$$C_c(\delta t) = \frac{\sum_i I_1(t_i) I_2(t_i + \delta t)}{\sqrt{\sum_i I_1(t_i)^2} \sqrt{\sum_i I_2(t_i + \delta t)^2}}, \tag{18}$$

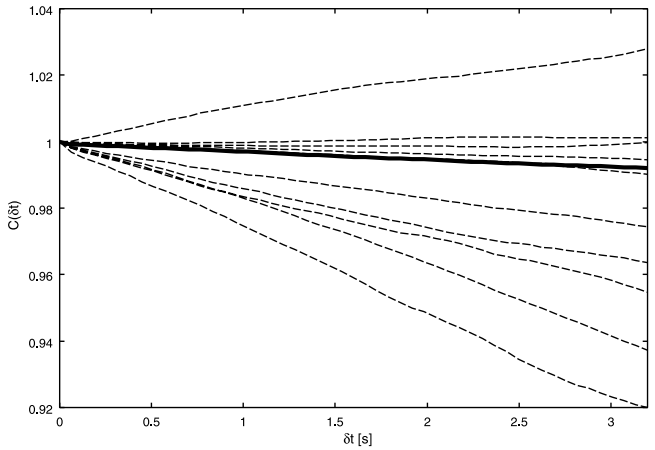

FIG. 10.—Autocorrelation for mock light curves. The thick solid curve is the autocorrelation for the original light curve (GRB 000421). Thin dashed curves are a portion of the autocorrelations for 2000 mock light curves based on the same GRB.

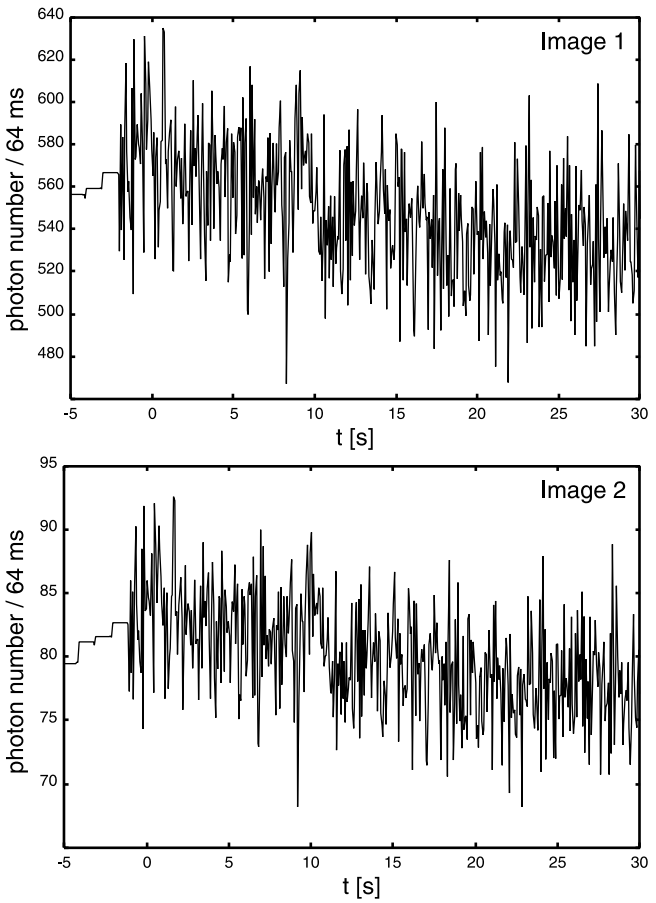

FIG. 11.—Decomposed light curves for GRB 940919, assuming that the observed light curve is the superposition of two lensed light curves with $\Delta t = 0.96$ s.

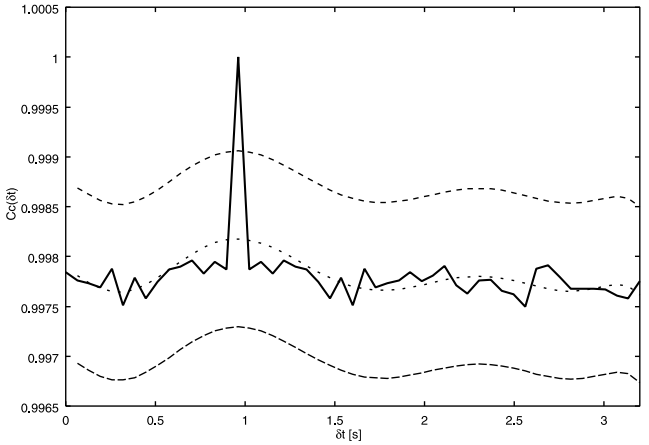

FIG. 12.—Cross-correlation of decomposed light curves shown in Fig. 11. The dotted line shows the best-fit curve, and dashed curves show $\pm 3\ \sigma$ levels. The cross-correlation shows a peak well above 3 σ, when δt is the same as $\Delta t = 0.96$ s.

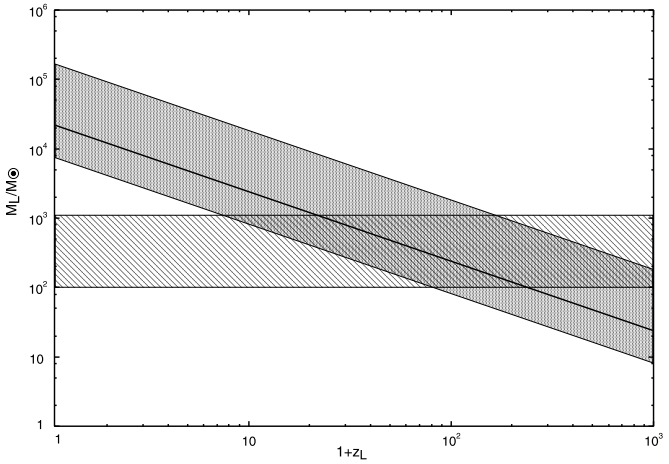

FIG. 13.—Dark gray region shows the suitable range of $M_L(1 + z_L)$ for GRB 940919. Here a 3 σ range of f (see Fig. 7*b*) is adopted. The central thick solid line corresponds to the case of $f = 1$, which is most probable. The hatched region is the mass range of Population III stars by Nakamura & Umemura (2001).

where δt is the time shift. The result is shown in Figure 12. As clearly shown in this figure, the cross-correlation is peaked when δt accords with $\Delta t = 0.96$ s. In addition, each decomposed light curve shows no bump higher than 3 σ in the autocorrelation for a reasonable range of f. Hence, we can conclude that the light curve of GRB 940919 is successfully decomposed and is likely to be the superposition of two lensed light curves.

4.4. *Redshift Estimation*

Here we constrain the redshift of the lens object. As shown in equation (7), Δt just determines $M_L(1 + z_L)$, except for f. If the probability density against f (Fig. 7*b*) is applied, we can derive a suitable range for $M_L(1 + z_L)$. The dark gray region in Figure 13 represents the suitable range for $\Delta t = 0.96$ s. On the other hand, the hatched region shows the mass range of Population III stars obtained by Nakamura & Umemura (2001). Combining these two regions, the allowed redshift of the lens object is at least $z_L \approx 10$. If $f = 1$ is adopted, the redshift ranges from $z_L \approx 20$ to $\approx$200, of which the most probable one is $z_L \approx 60$.

Nonetheless, there still exists another possibility that the lens object is as massive as $\sim 10^4\ M_\odot$ located at $z_L \simeq 0$, as seen in Figure 13. Loeb (1993) and Umemura et al. (1993) suggested that relic massive black holes are candidates for such an object. Sasaki & Umemura (1996) place a constraint on $\Omega_{\rm BH}$ from the UV background intensity and the Gunn-Peterson effect in the context of a cold dark matter cosmology. They find that the black hole mass density might be as low as $\Omega_{\rm BH}/\Omega_b \lesssim 10^{-3}$. Therefore, the expected incidence of bump detection for massive black holes is lower by 2 orders of magnitude than that for Population III stars.

5. CONCLUSIONS

To place constraints on the redshifts of GRBs that originate from Population III stars at $z > 10$, we have proposed a novel method based on gravitational lensing effects. If the lens is Population III stars with 10^2–$10^3\ M_\odot$ at $z > 10$, the time delay between two lensed images of a GRB is $\approx$1 s. This time delay is longer than the time resolution (64 ms) of GRB light curves and shorter than the duration of GRB events. Therefore, if a GRB is lensed, we observe the superposition of two lensed light curves. We have considered the autocorrelation method to extract the imprint of gravitational lensing by Population III stars in the GRB light curves. Using BATSE data, we have derived the probability of a resonance bump in the autocorrelation function, which is an indicator for the gravitational lensing. Applying this autocorrelation method to GRB light curves in the BATSE catalog, we have demonstrated that more than half of the light curves can show resonance bumps if they are lensed. Furthermore, in 1821 GRB light curves, we have found one candidate for a GRB lensed by a Population III star at $z \approx 60$. This method is quite straightforward and therefore provides an effective tool for searching for Population III stars at redshift greater than 10. Although the number of GRBs with available data is 1821 in this paper, the *Swift* satellite is now accumulating more GRB data. If this method is applied for those data, more candidates for GRBs lensed at $z > 10$ may be found in the future. These can provide firm evidence of massive Population III stars born at high redshifts.

We thank T. Murakami and D. Yonetoku for helpful information and fruitful discussion and S. Mao for his valuable comments. Numerical simulations were performed with facilities at the Center for Computational Sciences, University of Tsukuba. One of us (A. Y.) acknowledges the Japan Society for the Promotion of Science (09514), Inoue Foundation for Science, and JSPS Postdoctoral Fellowships for Research Abroad. This work was supported in part by Grants-in-Aid for Scientific Research from MEXT (16002003 to M. U.).

REFERENCES

Amati, L., et al. 2002, A&A, 390, 81
Andersen, M. I., et al. 2000, A&A, 364, L54
Baltz, E. A., & Hui, L. 2005, ApJ, 618, 403
Blaes, O. M., & Webster, R. L. 1992, ApJ, 391, L63
Bloom, J. S., Frail, D. A., & Kulkarni, S. R. 2003, ApJ, 594, 674
Bromm, V., & Loeb, A. 2002, ApJ, 575, 111
Fenimore, E. E., & Ramirez-Ruiz, E. 2000, ApJ, submitted (astro-ph/0004176)
Garnavich, P. M., Loeb, A., & Stanek, K. Z. 2000, ApJ, 544, L11
Gehrels, N., et al. 2004, ApJ, 611, 1005
Geiger, B., & Schneider, P. 1996, MNRAS, 282, 530
Heger, A., & Woosley, S. E. 2002, ApJ, 567, 532
Heger, A., et al. 2003, ApJ, 591, 288
Kawabata, K. S., et al. 2003, ApJ, 593, L19
Kawai, N. et al. 2006, Nature, 440, 184
Kogut, A., et al. 2003, ApJS, 148, 161
Koopmans, L. V. E., & Wambsganss, J. 2001, MNRAS, 325, 1317

Koshut, T. M., Paciesas, W. S., Kouveliotou, C., van Paradijs, J., Pendleton, G. N., Fishman, G. J., & Meegan, C. A. 1996, ApJ, 463, 570
Kouveliotou, C., et al. 1993, ApJ, 413, L101
Lamb, D. Q., & Reichart, D. E. 2000, ApJ, 536, 1
Lloyd-Ronning, N. M., Fryer, C. L., & Ramirez-Ruiz, E. 2002, ApJ, 574, 554
Loeb, A. 1993, ApJ, 403, 542
Loeb, A., & Perna, R. 1998, ApJ, 495, 597
Marani, G. F., Nemiroff, R. J., Norris, J. P., Hurley, K., & Bonnell, J. T. 1999, ApJ, 512, L13
Metzger, M., et al. 1997, Nature, 387, 879
Mizusawa, H., Nishi, R., & Omukai, K. 2004, PASJ, 56, 487
Murakami, T., Yonetoku, D., Umemura, M., Matsubayashi, T., & Yamazaki, R. 2005, ApJ, 625, L13
Nakamura, F., & Umemura, M. 2001, ApJ, 548, 19
Narayan, R., & Bartelmann, M. 1999, in Formation of Structure in the Universe, ed. A. Dekel & J. P. Ostriker (Cambridge: Cambridge Univ. Press), 360
Nemiroff, R. J., & Marani, G. F. 1998, ApJ, 494, L173
Nemiroff, R. J., et al. 1993, ApJ, 414, 36
Norris, J. P., Marani, G. F., & Bonnell, J. T. 2000, ApJ, 534, 248
Paczyński, B. 1986, ApJ, 308, L43
———. 1987, ApJ, 317, L51
Page, L., et al. 2006, ApJ, submitted (astro-ph/0603450)
Price, P. A., et al. 2003, Nature, 423, 844
Sasaki, S., & Umemura, M. 1996, ApJ, 462, 104
Schaefer, B. E., Deng, M., & Band, D. L. 2001, ApJ, 563, L123
Spergel, D., et al. 2003, ApJS, 148, 175
———. 2006, ApJ, submitted (astro-ph/0603449)
Turner, E. L., Ostriker, J. P., & Gott, J. R. 1984, ApJ, 284, 1
Turner, E. L., & Umemura, M. 1997, ApJ, 483, 603
Uemura, M., et al. 2003, Nature, 423, 843
Umemura, M., Loeb, A., & Turner, E. L. 1993, ApJ, 419, 459
Williams, L. L. R., & Wijers, R. A. M. J. 1997, MNRAS, 286, L11
Wyithe, J. S. B., & Turner, E. L. 2002, ApJ, 575, 650
Yonetoku, D., Murakami, T., Nakamura, T., Yamazaki, R., Inoue, A. K., & Ioka, K. 2004, ApJ, 609, 935